Check for updates

High Power Laser Science and Engineering, (2026), Vol. 14, e49, 6 pages.
doi:10.1017/hpl.2026.10141

HIGH POWER LASER SCIENCE AND ENGINEERING

RESEARCH ARTICLE

High-power InnoSlab amplifier with a multi-segmented composite Yb:YAG crystal

Yuguang Huang[1,2,3], Jie Guo[1], Wenhao Guo[1,4], Zichen Gao[1,2], Jinfeng Li[1], and Xiaoyan Liang[1]

[1]*State Key Laboratory of Ultra-intense Laser Science and Technology, Shanghai Institute of Optics and Fine Mechanics, Chinese Academy of Sciences, Shanghai, China*

[2]*Center of Materials Science and Optoelectronics Engineering, University of Chinese Academy of Sciences, Beijing, China*

[3]*Zhangjiang Laboratory, Shanghai, China*

[4]*School of Physical Science and Technology, ShanghaiTech University, Shanghai, China*

(Received 27 August 2025; revised 24 February 2026; accepted 10 April 2026)

Abstract

We demonstrate a high-power InnoSlab amplifier based on a multi-segmented composite ytterbium-doped yttrium aluminum garnet (Yb:YAG) crystal. A systematic comparison was performed of the laser amplification output performance of multi-segmented and conventional Yb:YAG crystals to demonstrate the feasibility of using gain media with multiple doping concentrations in InnoSlab laser amplifiers. We achieved an amplified output of 245 W based on the multi-segmented composite Yb:YAG crystal InnoSlab amplifier, with a beam quality of $M^2 = 1.21 \times 1.25$ and an optical-to-optical efficiency of 38.9%. Thanks to the unique doping structure of the composite crystal, compared to homogeneous dopant crystals, the average output power, optical-to-optical efficiency and beam quality were significantly improved. Exceptional output power stability with a root mean square fluctuation of 0.11% and pointing stability of approximately 7.5 μrad were achieved.

Keywords: high-power laser; InnoSlab amplifier; multi-segmented crystal; ytterbium-doped yttrium aluminum garnet

1. Introduction

Ultrafast lasers characterized by high average power and high repetition rates have been developed rapidly due to their significant applications in both scientific and industrial fields[1–3]. Considering the accompanying challenges is an essential aspect with the increasing output power. The wavefront distortion caused by uneven pump absorption degrades the beam quality of the amplification output. Among these challenges, thermal fracture represents the most significant limitation to power scaling. Increases in pumping power invariably result in rises in thermal stress, which may cause fracture at the maximum stress point[4]. The reduction of the temperature gradient within the crystal not only helps to prevent thermal fracture but also promises high beam quality output. InnoSlab amplifiers, renowned for their efficient thermal management and outstanding single-pass power amplification, have emerged as a highly efficient solution to achieve this goal[5–9]. Efficient heat dissipation is achieved due to the short distance between the pumped gain volume and the large cooled mounting surfaces. This effective heat dissipation also generates a one-dimensional heat flow inside the laser crystal, thus establishing a cylindrical thermal lens within the pumping volume of the gain medium[8]. Remarkable results, including output powers ranging from hundreds of watts to the kilowatt range[5,10–13], have demonstrated their significant potential.

Ytterbium-doped yttrium aluminum garnet (Yb:YAG) crystal is characterized by high quantum and Stokes efficiency, combined with excellent thermal conductivity. These properties position it as a highly suitable material for high-power laser systems, facilitating its extensive application in high-power lasers[10,11,14]. Conventional Yb:YAG crystals exhibit numerous advantageous properties; however, the pump absorption follows the Beer–Lambert law, resulting in the nonuniform distribution of pump energy along the propagation direction in conventional uniformly doped crystals. As the pump power is increased, the temperature gradient caused by nonuniform pump absorption produces pronounced thermal effects, which

Correspondence to: J. Guo and X. Liang, State Key Laboratory of Ultra-intense Laser Science and Technology, Shanghai Institute of Optics and Fine Mechanics, Chinese Academy of Sciences, Shanghai 201800, China. Emails: gracejie123@siom.ac.cn (J. Guo); liangxy@siom.ac.cn (X. Liang)

© The Author(s), 2026. Published by Cambridge University Press in association with Chinese Laser Press. This is an Open Access article, distributed under the terms of the Creative Commons Attribution-NonCommercial licence (https://creativecommons.org/licenses/by-nc/4.0), which permits non-commercial re-use, distribution, and reproduction in any medium, provided the original article is properly cited. The written permission of Cambridge University Press or the rights holder(s) must be obtained prior to any commercial use.

Downloaded from https://www.cambridge.org/core. 16 Nov 2026 at 16:45:44, subject to the Cambridge Core terms of use.

decrease the efficiency and beam quality, and also increase the potential risk of thermal fracture[15–17].

The composite crystal has been proven to effectively mitigate issues arising from the pump nonuniform absorption of a conventional uniformly doped crystal, thereby reducing the adverse effect of thermal load[18–21]. Jiang *et al.*[22] demonstrated the first multi-segmented neodymium-doped yttrium lithium fluoride (Nd:YLF) laser delivering a maximum continuous-wave (CW) output power of 35.5 W under a pump power of 105 W. The multi-segmented crystal was designed to straightforwardly aim for the minimum thermal stress without sacrificing the overall laser efficiency. The multi-segment and multi-concentration (MSMC) thulium-doped yttrium aluminum garnet (Tm:YAG) crystal was designed. The results showed that the MSMC structure can effectively alleviate the thermal effect of Tm:YAG crystal[23]. Shen *et al.*[24] designed a multi-segmented neodymium-doped yttrium orthovanadate (Nd:YVO_4) crystal and demonstrated a high-power all-solid-state laser emitting 10.0 W single-frequency radiation at 1342 nm. The optimized design displayed a two times lower thermal lens dioptric power compared to conventional crystal designs. Huang *et al.*[25] demonstrated a high-power master oscillator power amplifier with an output power of 108 W under a total incident pump power of 244 W based on the multi-segmented Nd:YVO_4 crystals. Experimental results revealed that the gain medium with multiple doping concentrations was practically valuable for constructing a high-power laser without bringing in significant thermal effects. Multi-segmented composite doped crystals, obtained by bonding crystals with different doping concentrations using a convenient fusion-bonding technology, are widely used for laser output[26–29]. No inorganic or organic bonding aid or adhesive is used during the crystal fabrication. The segment end-faces were precisely polished to a surface flatness of approximately λ/10, and after both the segments were optically contacted, they were heat-treated at a temperature a little below the crystal melting point to enhance bond strength[4]. A composite crystal with different doping concentrations provides more homogeneous pump absorption along the pump propagation direction, which helps to flatten the on-axis temperature and stress distributions[4,15,25,30]. The multi-segmented composite crystal facilitates the feasibility of laser amplification systems, producing superior beam quality and average power[23].

In this work, we report the first demonstration of the multi-segmented composite Yb:YAG InnoSlab laser amplifier, which can achieve high power amplification typically challenging to obtain using a single bulk crystal in other amplifier configurations. We have conducted a comprehensive comparison of the output performance of the composite and conventional Yb:YAG crystal InnoSlab amplifiers. The amplifier based on the composite crystal with multi-segmented doping concentrations of 2.0%, 3.0% and 2.0% delivers enhanced performance, providing higher power and superior beam quality amplification output. An amplified output of 245 W is achieved using the composite crystal, with a beam quality of $M^2 = 1.21 \times 1.25$ and an optical-to-optical efficiency of 38.9%. The laser system demonstrates notable output stability, with an output power root mean square (RMS) fluctuation as low as 0.11% and pointing stability of approximately 7.5 μrad.

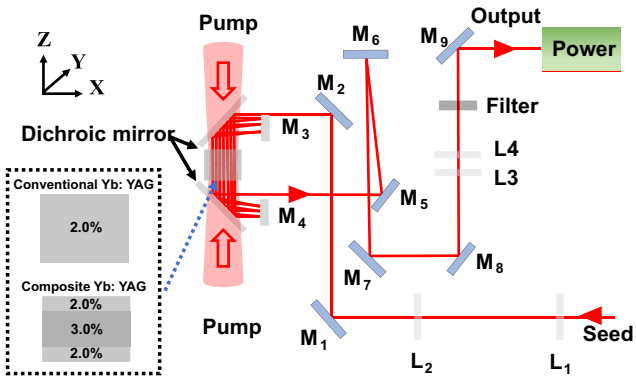


Figure 1. Schematic of the InnoSlab amplifier and crystal doping structure.

2. Experimental setup

The configuration of the InnoSlab laser amplifier is illustrated in Figure 1. Two CW laser diode stacks centered at 938 nm are used as pump sources. The pump radiation is reshaped by a series of lenses into a homogenous line of approximately 8 mm × 0.25 mm ($1/e^2$) with a total power of 630 W, characterized by a top-hat intensity distribution along the slow axis (*X*-direction) and a Gaussian intensity distribution along the fast axis (*Y*-direction) with a Rayleigh length of 8 mm. The polarization of the pump radiation is along the *Y*-direction. A 2%-doped Yb:YAG crystal grown in-house with dimensions of 10 mm × 12 mm × 1 mm is used as the gain medium. The two 12 mm × 1 mm end-faces are antireflection-coated at 940 and 1030 nm and serve as the pump incidence surfaces, while the two 10 mm × 12 mm surfaces are clamped to a custom-designed, water-cooled copper heat sink, ensuring efficient thermal management. A dual-end and dual-pass pump geometry is employed here to improve the pump absorption and intensity through polarization control by means of thin film polarizers (TFPs), a half wave plate (HWP) and reflective mirrors[10]. For a single-pass pump, the laser medium demonstrates an absorption efficiency of 62%, whereas in the configuration of the double-pass pump, the crystal achieves a single-pass small-signal gain of 1.9.

A convex cylindrical mirror M_3 with a radius of curvature of 700 mm and a plane mirror M_4, both coated for high reflectivity at 1030 nm for 0° incidence, with the

Downloaded from https://www.cambridge.org/core. 16 Nov 2026 at 16:45:44, subject to the Cambridge Core terms of use.

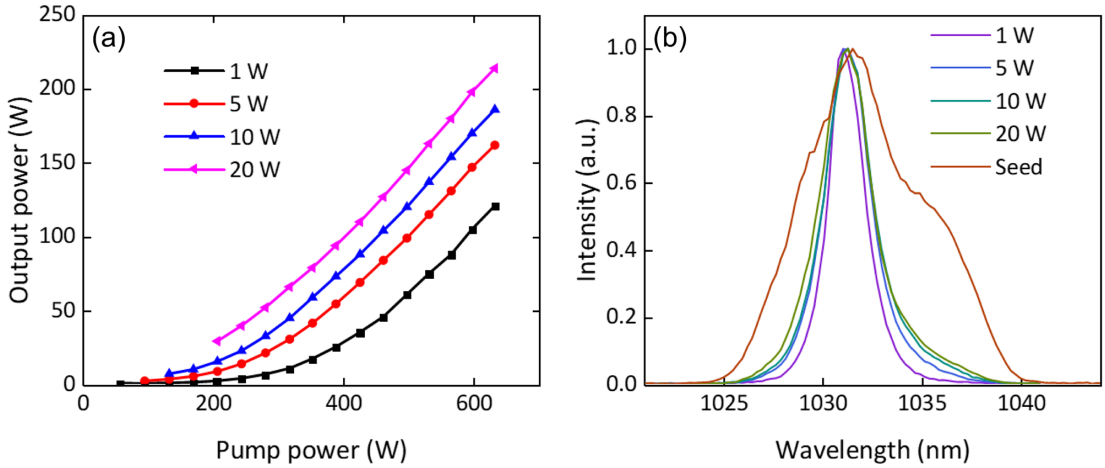


Figure 2. (a) Output power versus incident pump power for different injection seed power levels of the Yb:YAG amplifier. (b) Seed and amplifier output spectra for different injection seed power levels of the Yb:YAG amplifier.

diameter of 0.5 inch and a damage threshold of 1 J/cm^2, form the amplification cavity with a length of 65 mm, ensuring efficient mode matching. Two dichroic mirrors are positioned between the mirrors and the crystal to guarantee that the pump passes through the medium while facilitating six internal reflections of the seed, creating a seven-pass amplifier configuration. The dichroic mirrors are 45° antireflective-coated at 940 nm and highly reflective-coated at 1030 nm. The seed is provided by a commercial all-fiber laser (Amplitude, Tangerine), with a central wavelength of 1032 nm, a bandwidth of $\Delta\lambda = 8.3$ nm and a chirped pulse duration of about 500 ps at a repetition rate of 175 kHz. After passing through an optical isolator, the seed is shaped via two spherical lenses L_1 and L_2 (both with a focal length of 200 mm) and coupled into the amplifier. The shaped beam waist has a diameter of $2\omega_0 = 260$ μm, with the waist position at the cavity mirror M_3.

To facilitate succeeding application experiments, further beam shaping and spatial filtering are implemented. The amplified output is transformed into a circular beam by a spherical mirror M_6 with a radius of curvature of –400 mm and two cylindrical lenses L_3 and L_4 (both with a focal length of 150 mm). A water-cooled pinhole, positioned at the beam focus, is used as a spatial filter, which improves the beam quality but introduces a power loss of approximately 6.4%.

3. Results and discussion

Figure 2(a) illustrates the amplified output versus the incident pump power for different injection seed levels (1, 5, 10 and 20 W). A maximum output power of 211 W is achieved with an injection seed power of 20 W at the pump power of 630 W after seven-pass amplification, corresponding to an optical-to-optical efficiency of 33.4%. The spectral characteristics of both the injected seed and the amplified output for different seed power levels, at the pump power of 630 W, are depicted in Figure 2(b). The full width at half maximum (FWHM) spectral bandwidth of $\Delta\lambda = 8.3$ nm from the front end is reduced to 3.1 nm. Increasing the seed power results in a slightly broader output spectral bandwidth, because lower injection seed powers experience a higher amplification gain, intensifying gain narrowing. The seed laser is centered at 1032 nm, while the amplified output exhibits a blue-shifted central wavelength of 1031 nm, corresponding to the stimulated emission center wavelength of Yb:YAG crystals. Detailed characteristics of the beam profile were analyzed using Ophir's beam quality analyzer (Ophir BeamSquared, BSQ-SP920), facilitating the measurement of the beam quality at a maximum output power of 211 W. The filtered beam quality of the output, characterized by the beam quality factors $M_x^2 = 1.34$ and $M_y^2 = 1.23$ in the two orthogonal directions, is presented in Figure 3, while a beam quality factor of $M^2 = 1.41 \times 1.30$ is recorded when not filtered.

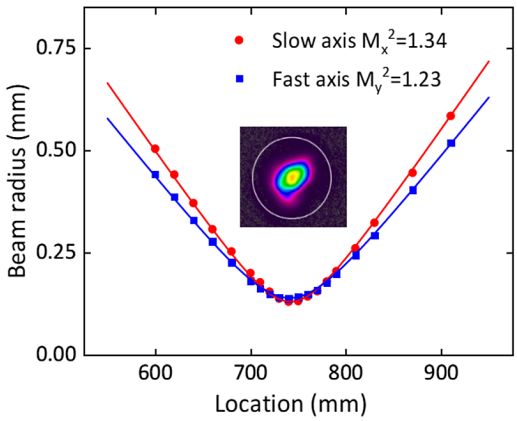


Figure 3. Output beam quality of the Yb:YAG amplifier measured with a commercial instrument (Ophir BeamSquared, BSQ-SP920). The inset displays the near-field beam profile.

Downloaded from https://www.cambridge.org/core. 16 Nov 2026 at 16:45:44, subject to the Cambridge Core terms of use.

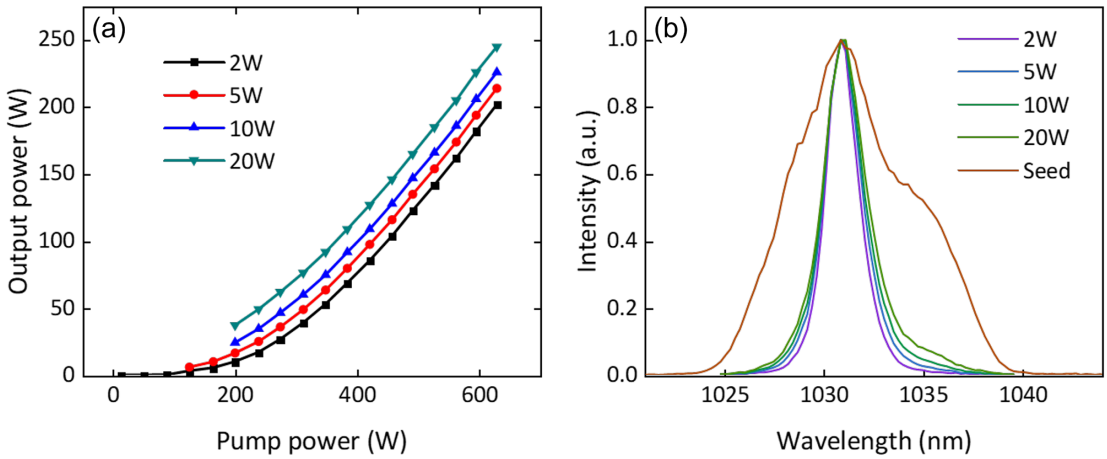


Figure 4. (a) Output power versus incident pump power for different injection seed power levels of the composite Yb:YAG amplifier. (b) Seed and amplifier output spectra for different injection seed power levels of the composite Yb:YAG amplifier.

In the following experiments, the multi-segmented composite Yb:YAG crystal is employed to achieve higher amplification output power with high beam quality. In Figure 1, the schematic of the doping structure of the composite Yb:YAG crystal is presented. The crystal implemented in this section has augmented the doping concentration in the middle segment. The crystal features a doping concentration layout of 2% + 3% + 2%, with dimensions of 10 (2.5 + 5.0 + 2.5) mm × 12 mm × 1 mm correspondingly. Within such a doping configuration, the crystal exhibits an equivalent doping concentration of 2.5%, and through simulation analysis, a relatively uniform temperature distribution can be achieved. In the simulation, the heat source distribution within the crystal can be determined according to the distribution characteristics of the pump in the crystal, and the crystal temperature distribution can be obtained based on the finite element analysis. It is noteworthy that this simulation model can be referred to in Ref. [9]. This doping concentration design has the potential to enhance the efficiency of pump absorption and promote more uniform pump energy distribution, thus facilitating high-power and high beam quality laser amplification. For a single pump pass, the crystal achieves an absorption efficiency of 73.3%, while the single-pass small-signal gain in the double-pass pump reaches 3.4. The two critical values are notably higher than those of the conventional Yb:YAG crystal employed in the earlier analysis, paving the way for the subsequent enhancement of amplified output power.

The output power as a function of pump power for different injection seed levels (2, 5, 10 and 20 W) is characterized, as shown in Figure 4(a). With 20 W seeding, a maximum output power of 245 W is obtained at the pump power of 630 W, corresponding to an optical-to-optical efficiency of 38.9%. The single-pass small-signal gain demonstrates a notable enhancement, increasing from 1.9 of the conventional Yb:YAG crystal to 3.4 of the composite Yb:YAG crystal, enabling higher amplification under identical pump and seed conditions. The output power improves from 211 to 245 W, while the optical-to-optical efficiency increases from 33.4% to 38.9%. The high gain capability also produces 210 W output power from only 1 W injection seed, a feature particularly advantageous for amplifiers operating with low-power seed sources. Figure 4(b) shows the pulse spectra of both the injected seed and amplified output at different seed power levels at 630 W pump power. The stretched pulse seeding the amplifier has a spectral bandwidth of 8.3 nm, which is subsequently reduced by the gain-narrowing effect to 2.4 nm. With an increased injection seed power, the spectral bandwidth of the output is broadened from 1.9 nm at 2 W injection seed to 2.4 nm at 20 W injection seed.

For the composite crystal, the amplifier output beam quality is characterized as $M^2 = 1.21 \times 1.25$ at a pump power of 630 W and output power of 245 W, as illustrated in Figure 5. The beam quality without filtering was measured to be $M^2 = 1.39 \times 1.29$. Compared with the conventional Yb:YAG amplifier, the composite crystal produces a more regular output beam profile, owing to the more uniform pump distribution and temperature field. The beam quality is improved, and the beam modes in both orthogonal directions are more consistent.

As illustrated in Figure 6, the output power of the composite crystal is compared to that of the conventional Yb:YAG crystal at a series of injection seed powers, with a constant pump power of 630 W. At equivalent levels of injection seed, the composite crystal demonstrates considerably higher output powers in comparison to the conventional Yb:YAG crystal, a phenomenon attributable to higher pump absorption and single-pass gain. This phenomenon is particularly notable at lower injection seed powers, where a more pronounced slope is exhibited in the output power curve of the conventional Yb:YAG crystals. With the enhancement

Downloaded from https://www.cambridge.org/core. 16 Nov 2026 at 16:45:44, subject to the Cambridge Core terms of use.

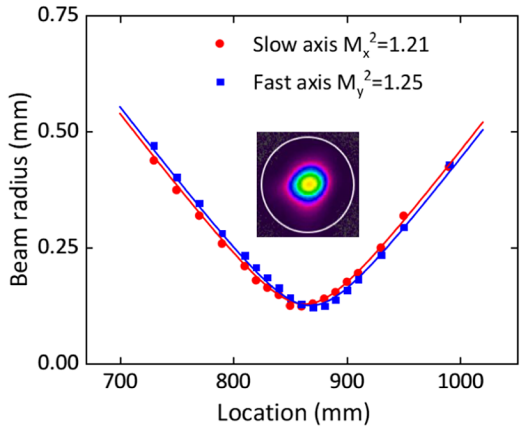


Figure 5. Output beam quality of the composite Yb:YAG amplifier measured with a commercial measurement device.

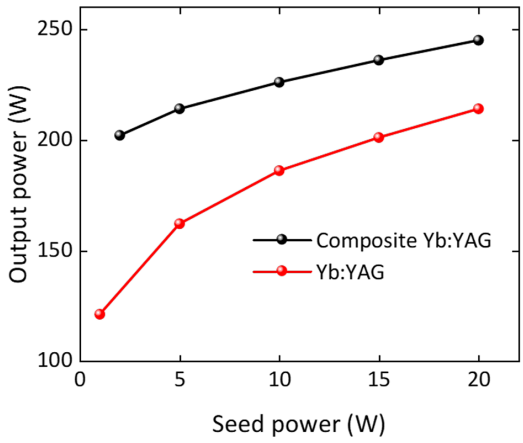


Figure 6. Output power of the conventional Yb:YAG and composite Yb:YAG amplifiers with different injection seed power.

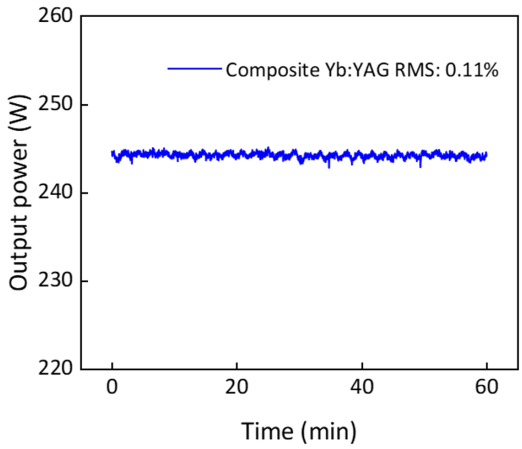


Figure 7. Output power stability of the composite Yb:YAG amplifier in 1 hour.

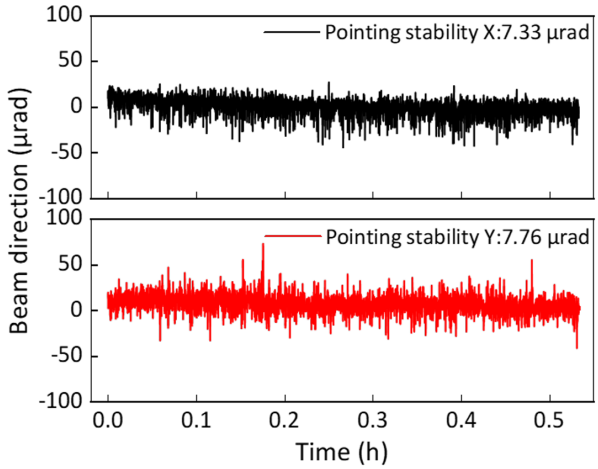


Figure 8. Output pointing stability of the composite Yb:YAG amplifier.

of the injection seed power, the discrepancy between the two gradually mitigates. This phenomenon corresponds to an elevated extraction of energy from the upper energy level of the crystals, giving rise to a corresponding reduction in the disparity between the two crystals. Upon reaching approximately 15 W of injection seed, the slopes of the output power curves for both crystals exhibit a notable decrease, indicating saturation of the laser output.

The laser system demonstrates notable stability with respect to both output power and pointing. The output power stability is measured with RMS fluctuations as low as 0.11% over a 1-hour period, as shown in Figure 7. The maximum and minimum output powers during the testing period are 245 and 243 W, respectively. A 30-minute test on the output pointing is also conducted, and the details are presented in Figure 8. The output pointing values of the composite crystal in the *X* and *Y* directions are measured to be 7.33 and 7.76 μrad, respectively. Improving the stability of both the output power and the pointing allows this amplifier to be applied more effectively as a component source in coherent beam combining and a driving source for high-flux high-order harmonic generation if combined with post-compression.

4. Summary

In this paper, we have demonstrated the multi-segmented composite Yb:YAG (2.0% + 3.0% + 2.0%) InnoSlab laser amplifier delivering an average output power of 245 W from a 20 W injection seed at 175 kHz, achieving an optical-to-optical efficiency of 38.9%. The high single-pass small-signal gain of 3.4 enables the production of 210 W amplified output from only a 1 W injection seed, making this configuration particularly beneficial for low-power seed sources. In addition, the laser exhibited excellent beam quality, $M^2 = 1.21 \times 1.25$. We significantly boosted the output efficiency, output power and beam quality of the composite crystal compared to the laser amplification output of the conventional Yb:YAG crystal, with the output power of 211 W from a 20 W injection seed, the optical-to-optical efficiency of 33.4% and the beam quality of 1.34 × 1.23. The

Downloaded from https://www.cambridge.org/core. 16 Nov 2026 at 16:45:44, subject to the Cambridge Core terms of use.

composite Yb:YAG crystal amplifier demonstrates excellent output stability, with an output power RMS fluctuation as low as 0.11% and pointing stabilities of 7.33 and 7.76 μrad, respectively. Improving the stability of both the output power and the pointing allows this amplifier to be applied more effectively as a component source in coherent beam combining and a driving source for nonlinear optics applications. In this work, the enhanced laser amplification performance achieved based on the composite Yb:YAG crystal highlights the promising potential of the composite crystal for efficient high-power pulse amplification.

Acknowledgements

This work was supported by the Program of Shanghai Academic/Technology Research Leader (Grant No. 20SR014501) and Zhangjiang Laboratory.

References

1. P. L. Kramer, M. K. R. Windeler, K. Mecseki, E. G. Champenois, M. C. Hoffmann, and F. Tavella, Opt. Express **28**, 16951 (2020).
2. I. Mingareev, N. Bautista, D. Yadav, and A. Bhanderi, Opt. Laser Technol. **160**, 109078 (2023).
3. A. L. Viotti, M. Seidel, E. Escoto, S. Rajhans, W. P. Leemans, I. Hartl, and C. M. Heyl, Optica **9**, 197 (2022).
4. M. Tsunekane, N. Taguchi, T. Kasamatsu, and H. Inaba, IEEE J. Sel. Top. Quantum Electron. **3**, 9 (1997).
5. P. Russbueldt, T. Mans, G. Rotarius, J. Weitenberg, H. D. Hoffmann, and R. Poprawe, Opt. Express **17**, 12230 (2009).
6. P. Russbueldt, D. Hoffmann, M. Höfer, J. Lohring, J. Luttmann, A. Meissner, J. Weitenberg, M. Traub, T. Sartorius, D. Esser, R. Wester, P. Loosen, and R. Poprawe, IEEE J. Sel. Top. Quantum Electron. **21**, 447 (2014).
7. J. Guo, H. Lin, J. Li, P. Gao, and X. Liang, Opt. Lett. **41**, 2875 (2016).
8. J. Guo, L. Guo, Z. Gao, Y. Gao, Z. Gan, Y. Huang, X. Liang, and R. Li, Opt. Lett. **49**, 4385 (2024).
9. Y. Huang, J. Guo, J. Li, Z. Gao, and X. Liang, Opt. Commun. **583**, 131794 (2025).
10. Y. Gao, J. Guo, Z. Gao, Y. Huang, Z. Tu, and X. Liang, Opt. Laser Technol. **168**, 109885 (2024).
11. Y. Gao, J. Guo, Y. Huang, Z. Gao, Z. Gan, Z. Tu, X. Liang, and R. Li, Opt. Lett. **48**, 5328 (2023).
12. P. Russbueldt, T. Mans, J. Weitenberg, H. D. Hoffmann, and R. Poprawe, Opt. Lett. **35**, 4169 (2010).
13. P. Russbueldt, J. Weitenberg, J. Schulte, R. Meyer, C. Meinhardt, H. D. Hoffmann, and R. Poprawe, Opt. Lett. **44**, 5222 (2019).
14. C. Wang, J. B. Khurgin, and H. Yu, Opt. Lett. **48**, 5751 (2023).
15. Y. Huang and Y. Chen, Opt. Express **21**, 16063 (2013).
16. X. Chen, L. Xu, H. Hu, T. Zhou, Y. Sun, H. Jiang, J. Lei, W. Lv, H. Su, Y. Shi, M. Li, Y. Wu, Z. Yao, N. Zhao, X. Xu, Q. Gao, X. Wang, and C. Tang, Opt. Express **24**, 24517 (2016).
17. S. C. Tidwell, J. F. Seamans, M. S. Bowers, and A. K. Cousins, IEEE J. Quantum Electron. **28**, 997 (1992).
18. J. Liu, Y. Wen, S. Li, L. Gong, C. Wu, Y. Yu, C. Wang, and G. Jin, Opt. Commun. **480**, 126452 (2021).
19. C. Evangelatos, G. Tsaknakis, P. Bakopoulos, D. Papadopoulos, G. Avdikos, A. Papayannis, and G. Tzeremes, IEEE Photon. Technol. Lett. **26**, 1890 (2014).
20. Y. Huang, Y. Huang, H. Liang, K. Su, Y. Chen, and K. Huang, Opt. Express **18**, 9518 (2010).
21. Y. Chang, Y. Huang, K. Su, and Y. Chen, Opt. Express **16**, 21155 (2008).
22. C. Jiang, W. Huang, Q. He, J. He, S. Zhu, H. Yin, Z. Li, Z. Chen, and S. Dai, Opt. Lett. **48**, 799 (2023).
23. J. Dong, J. Cui, Y. Wen, C. Wu, and C. Wang, Infrared Phys. Techn. **122**, 104104 (2022).
24. Q. Shen, X. Y. Cui, M. C. Yan, U. Eismann, T. Yuan, W. Z. Zhang, C. Z. Peng, Y. A. Chen, and J. W. Pan, Opt. Express **27**, 31913 (2019).
25. Y. J. Huang, W. Z. Zhuang, K. W. Su, and Y. F. Chen, IEEE J. Sel. Top. Quantum Electron. **21**, 226 (2014).
26. A. M. Rodin, M. Grishin, and A. Michailovas, Opt. Laser Technol. **76**, 46 (2016).
27. R. Wilhelm, D. Freiburg, M. Frede, D. Kracht, and C. Fallnich, Opt. Express **17**, 8229 (2009).
28. D. Kracht, R. Wilhelm, M. Frede, K. Dupré, and L. Ackermann, Opt. Express **13**, 10140 (2005).
29. D. Chen, X. Li, Y. Zhang, X. Yu, F. Chen, R. Yan, Y. Ma, and C. Wang, Laser Phys. Lett. **8**, 46 (2011).
30. R. Wilhelm, M. Frede, and D. Kracht, IEEE J. Quantum Electron. **44**, 232 (2008).

Downloaded from https://www.cambridge.org/core. 16 Nov 2026 at 16:45:44, subject to the Cambridge Core terms of use.